ISSN 1674-1056
http://cpb.iphy.ac.cn
http://iopscience.iop.org/cpb
中国物理 B
Chinese Physics
中国物理 Chinese Physics B

# First-principles investigations of proton generation in *α*-quartz

Yunliang Yue(乐云亮), Yu Song(宋宇), Xu Zuo(左旭)
**Citation:**Chin. Phys. B . 2018, 27(3): 037102. **doi:** 10.1088/1674-1056/27/3/037102

Journal homepage: http://cpb.iphy.ac.cn; http://iopscience.iop.org/cpb

**What follows is a list of articles you may be interested in**

---

## Uniaxial strain-modulated electronic structures of Cd*X* (*X*=S, Se, Te) from first-principles calculations: A comparison between bulk and nanowires

Linlin Xiang(相琳琳), Shenyuan Yang(杨身园)
Chin. Phys. B . 2017, 26(8): 087103. **doi:** 10.1088/1674-1056/26/8/087103

## Effect of anionic ordering on the electronic and optical properties of $BaTaO_2N$: TB-mBJ density functional calculation

K Bettine, O Sahnoun, M Sahnoun, M Driz
Chin. Phys. B . 2017, 26(5): 057101. **doi:** 10.1088/1674-1056/26/5/057101

## Electrical property effect of oxygen vacancies in the heterojunction of $LaGaO_3/SrTiO_3$

Fu-Ning Wang(王芙凝), Ji-Chao Li(李吉超), Xin-Miao Zhang(张鑫淼), Han-Zhang Liu(刘汉璋), Jian Liu(刘剑), Chun-Lei Wang(王春雷), Ming-Lei Zhao(赵明磊), Wen-Bin Su(苏文斌), Liang-Mo Mei(梅良模)
Chin. Phys. B . 2017, 26(3): 037101. **doi:** 10.1088/1674-1056/26/3/037101

## Structural, electronic, and magnetic properties of vanadium atom-adsorbed $MoSe_2$ monolayer

Ping Liu(刘萍), Zhen-Zhen Qin(秦真真), Yun-Liang Yue(乐云亮), Xu Zuo(左旭)
Chin. Phys. B . 2017, 26(2): 027103. **doi:** 10.1088/1674-1056/26/2/027103

## Band offsets engineering at $Cd_xZn_{1-x}S/Cu_2ZnSnS_4$ heterointerface

Wujisiguleng Bao(包乌吉斯古楞), Sachuronggui(萨初荣贵), Fang-Yuan Qiu(仇方圆)
Chin. Phys. B . 2016, 25(12): 127102. **doi:** 10.1088/1674-1056/25/12/127102

---

# First-principles investigations of proton generation in $\alpha$-quartz*

Yunliang Yue(乐云亮)[1], Yu Song(宋宇)[2,3], and Xu Zuo(左旭)[1,4,†]

[1] College of Electronic Information and Optical Engineering, Nankai University, Tianjin 300071, China
[2] Microsystem and Terahertz Research Center, China Academy of Engineering Physics, Chengdu 610200, China
[3] Institute of Electronic Engineering, China Academy of Engineering Physics, Mianyang 621999, China
[4] Municipal Key Laboratory of Photo-electronic Thin Film Devices and Technology, Nankai University, Tianjin 300071, China

(Received 19 October 2017; revised manuscript received 7 December 2017; published online 11 February 2018)

Proton plays a key role in the interface-trap formation that is one of the primary reliability concerns, thus learning how it behaves is key to understand the radiation response of microelectronic devices. The first-principles calculations have been applied to explore the defects and their reactions associated with the proton release in $\alpha$-quartz, the well-known crystalline isomer of amorphous silica. When a high concentration of molecular hydrogen ($H_2$) is present, the proton generation can be enhanced by cracking the $H_2$ molecules at the positively charged oxygen vacancies in dimer configuration. If the concentration of molecular hydrogen is low, the proton generation mainly depends on the proton dissociation of the doubly-hydrogenated defects. In particular, a fully passivated $E_2'$ center can dissociate to release a proton barrierlessly by structure relaxation once trapping a hole. This research provides a microscopic insight into the proton release in silicon dioxide, the critical step associated with the interface-trap formation under radiation in microelectronic devices.

**Keywords:** first-principles calculation, interface trap, proton, silicon dioxide

**PACS:** 71.15.Mb, 71.20.–b, 61.72.Bb, 61.80.Az **DOI:** 10.1088/1674-1056/27/3/037102

## 1. Introduction

Radiation-induced silicon/silica interface traps are the dominant defects associated with the reliability of microelectronic devices.[1–4] The mechanisms leading to the interface-traps have been extensively studied, where hydrogen plays a crucial role. It has been shown that both interface and oxide charge buildups induced by radiation increase with the increasing hydrogen amount exposed during processing, indicating that hydrogen can facilitate the interface trap generation and enhance the degradation of microelectronic devices.[5–7] In fact, hydrogen can play a double role. On one hand, it can passivate or anneal the interface dangling bonds, the dominant interface traps,[8] if its concentration and form near the interface are appropriate. On the other hand, it can react with the interface dangling bonds previously passivated by hydrogen and reactivate them. The reactions giving rise to the interface dangling bond have also been intensively studied, and it has been shown by first-principles calculations that protons generated by ionization radiation can attack the Si–H bonds, the passivated dangling bonds, at the interface to reactivate the interface trap with a low reaction barrier.[9,10] The radiation-induced proton release is thus directly correlated to the interface trap reactivation. In fact, since the proton release and transportation are generally slow, they may contribute to the enhanced low dose rate sensitivity (ELDRS).[11–13]

Several mechanisms have been proposed for proton release from different sources in silica. A mechanism is the dissociation of $H_2$ molecules at the positively charged oxygen deficiency defects,[14,15] such as $E_\delta'$ and $E_\gamma'$ centers, which has been investigated by first-principles calculations.[16–18] It has been shown that $H_2$ molecules react with these positively charged defects, producing protons and neutral hydrogenated defects. This mechanism tends to be dominant if there is a sufficient supply of $H_2$ molecules, which can be the residue of hydrogen exposed in processing. Another mechanism is the dissociation of hydrogenated defects after trapping holes. It has been shown that the passively charged singly or doubly hydrogenated oxygen deficient defects can release protons and restore neutral charge state.[19] Hydrogen annealing of the interface dangling bonds can also anneal the oxygen vacancies that are abundant in silica, leading to the hydrogenated defects.

Although the proton release reactions in amorphous silica (a-$SiO_2$) have been investigated by first-principles calculations, the calculated reaction curves depend on the local environments, which are different site-by-site. Thus, the reaction barriers and energies calculated using a-$SiO_2$ models are usually scattered, leading to uncertainties in further numerical simulations based on drift-diffusion equations, where they are the fixed parameters. The calculations using a crystalline isomer of $SiO_2$ can detour this difficulty. In fact, all the defect centers involved in the proton release reactions in a-$SiO_2$ have their counterparts in quartz, the well-studied crystalline

*Project supported by the Science Challenge Project, China (Grant No. TZ2016003-1-105), CAEP Microsystem and THz Science and Technology Foundation, China (Grant No. CAEPMT201501), the National Natural Science Foundation China (Grant No. NSFC 11404300), and the National Basic Research Program of China (Grant No. 2011CB606405).

†Corresponding author. E-mail: xzuo@nankai.edu.cn

© 2018 Chinese Physical Society and IOP Publishing Ltd 

$SiO_2$. For example, the $E'_\gamma$ center in a-$SiO_2$ corresponds to the $E'_1$ center in quartz, and the singly hydrogenated oxygen vacancy in a-$SiO_2$ can be mapped to the $E'_2$ or $E'_4$ in quartz. More than that, the microscopic structures of these $E'$ centers have been reliably specified by the electron paramagnetic resonance (EPR) measurements.[20–23] We thus take $\alpha$-quartz to model the proton release reactions in a-$SiO_2$.[24]

In this work, the first-principles calculations are taken to investigate the defects and reactions associated with two proton release mechanisms, the dissociation of molecular hydrogen at a positively charged defect and that of a hydrogenated defect after trapping a hole. The structures, density of states (DOS), and spin densities are calculated for the defects, and also the Fermi contacts for the EPR-active ones. The reaction barriers and energies, the key parameters in further numerical simulations based on drift-diffusion equations, are extracted from the calculated reactions curves. The crystalline structure of quartz significantly reduces the uncertainty of the calculation due to the randomness of a-$SiO_2$, which is helpful to identify and characterize atomic scale mechanisms for radiation-induced proton release.

## 2. Methods

The calculations have been performed in the framework of density functional theory (DFT) with the projected augmented wave method implemented in the Vienna *ab initio* simulation package (VASP).[25–27] The Perdew–Burke–Ernzerhof (PBE) parameterization of general gradient approximation (GGA) is chosen for the exchange–correlation functional.[28] The cut-off energy of plane wave expansion is set to be 520 eV. The experimental lattice parameters,[29] $a = 4.916$ Å and $c = 5.4054$ Å, are set for the initial quartz unit cell. The $2\times2\times3$ supercells including 108 atoms are constructed for the calculations. The Brillouin zone integration is taken only at the $\Gamma$-point. The structure optimization will continue until the total energy difference between consecutive cycles is less than $10^{-4}$ eV and the force on each atom is less than 0.05 eV/Å. The partial occupancies are determined by using the Gaussian smearing scheme with a smearing width of 0.1 eV. The climbing image nudged elastic band (CI-NEB) method that couples a series of DFT calculations is applied to calculate the reaction curves.[30] Images are inserted to search for the minimum-energy path and the saddle point between the initial state (IS) and the final state (FS), and the spring constant is set to be 5.0 eV/Å$^2$ between adjacent images. The (forward) reaction barrier is defined by $E_{\rm bar} = E_{\rm TS} - E_{\rm IS}$, where $E_{\rm TS}$ and $E_{\rm IS}$ are the total energies of transient and initial states, respectively. The reaction energy is defined by $\Delta E = E_{\rm FS} - E_{\rm IS}$, where $E_{\rm FS}$ and $E_{\rm IS}$ are the total energies of final and initial states, respectively. To reproduce the bandgap underestimated by the exchange-correlations based on local density approximation including GGA, the electronic structures of the defects are specially calculated by using the unscreened hybrid functional where the Hartree–Fock exchange is mixed with PBE at 35%.[31] Spin-polarization is enabled in all calculations to describe the unpaired electrons properly.

## 3. Results and discussion

Holes play a crucial role in the mechanisms of radiation-induced proton release. They are induced as electron–hole pairs in the oxide by ionization radiation, and then transport with a rather low mobility compared to electrons, since they tend to trap themselves by distorting the lattice. The holes that survive from the initial recombination may be trapped by neutral oxygen vacancies, the most abundant defect in oxygen deficiency silica. This leads to the positively charged configurations, such as dimer ($E'_\delta$) and puckered ($E'_\gamma$) configurations in a-$SiO_2$, which may react with $H_2$ molecules to give rise to protons.[32] This mechanism however requires a sufficient supply of $H_2$, which can also be radiolytic. The holes may also be trapped by the hydrogenated defects, and then the positively charged hydrogenated defects dissociate to give protons. This mechanism requires pre-existing hydrogenated defects, which can be generated in the hydrogen annealing of interface traps.

### 3.1. Positively charged oxygen deficiency defects

It is necessary to specify the structure and other properties of the positively charged oxygen deficiency defects in quartz before the simulation of $H_2$ dissociation at the defects.[24,33] Since both quartz and a-$SiO_2$ are networks of $SiO_4$ building blocks, it is reasonable to assume that the most prevalent positively charged oxygen deficiency defects in quartz are analogous to those in a-$SiO_2$. Two configurations of positively charged oxygen vacancies in quartz are considered in the calculations. One is the dimer configuration, analogous to the $E'_\delta$ center in a-$SiO_2$, and the other is the well-known $E'_1$ center,[34] corresponding to the $E'_\gamma$ center in a-$SiO_2$. The $E'_1$ and $E'_\gamma$ centers are characterized by the puckered configuration, where a Si atom adjacent to the oxygen vacancy relaxes backward through its basal oxygen plane and bonds to a back oxygen atom, leading to a Si dangling bond and a three-coordinated oxygen.

The dimer configuration can be obtained by optimizing the initial structure, where the oxygen vacancy is induced by removing an oxygen atom and the hole-trapping is simulated by removing an electron. A perturbation to the initial structure is however required to obtain the puckered configuration, since there is an energy barrier between the initial structure and the puckered configuration. In spite of the barrier, the puckered configuration is energetically more stable than the dimer by 133 meV.

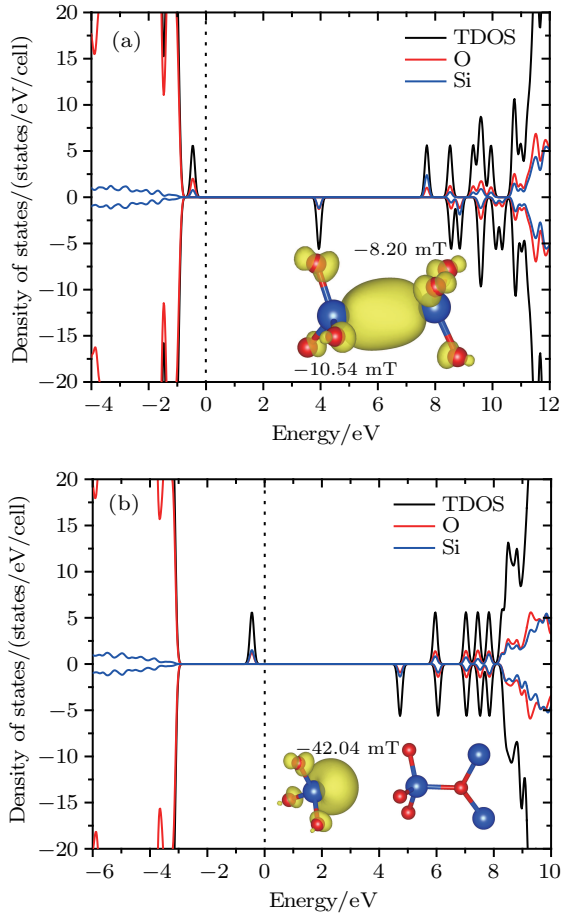



**Fig. 1.** (color online) The calculated DOS of (a) the dimer configuration and (b) the puckered configuration ($E_1'$) of the positively charged oxygen vacancy in $\alpha$-quartz, where the structures and spin densities are shown in the insets, respectively.

The atomic structure of the dimer configuration is presented in the inset of Fig. 1(a). The Si–Si bond over the vacancy in the dimer configuration is 2.95 Å, which is longer than that in a neutral oxygen vacancy and in good accordance with the previous report.[35] The total magnetic moment is 1.0 $\mu_B$, and the spin density asymmetrically distributes between the two Si atoms adjacent to the vacancy. The asymmetry of the spin density is confirmed by the calculated Fermi contacts on the two Si atoms, which are −10.54 mT and −8.20 mT, respectively. The asymmetry is associated with the quartz structure, where the two bonds of each oxygen atom are unequal. The calculated DOS shows that there is an occupied shallow state in the spin-up channel at 0.26 eV above the valence band maximum (VBM) and an unoccupied deep state in the spin-down channel at 4.67 eV above the VBM. The calculated DOS implies that the dimer configurations are not deep hole traps, and may exchange the captured holes with the lattice.

The structure of the puckered configuration ($E_1'$) is presented in the inset of Fig. 1(b). The puckering significantly increases the Si–Si distance over the vacancy to 4.29 Å, which is much larger than the Si–Si bond length in the neutral oxygen vacancy. The total magnetic moment is 1.0 $\mu_B$, and the spin density is almost entirely localized on the three-coordinated Si atom. A large Fermi contact of −42.04 mT on the three-coordinated Si atom is consistent with the spin density and in excellent agreement with the electron spin resonance measurements in $\alpha$-quartz.[36] The calculated DOS shows that the occupied and unoccupied states are at 2.46 eV and 7.64 eV above the VBM, respectively, implying that the puckered configuration is a deep hole trap.

### 3.2. Reactions between $H_2$ and the dimer or puckered configuration

The dissociation of $H_2$ at the dimer configuration is investigated by the NEB calculations, which gives the reaction curve connecting the initial and final states and the transition state associated with the energy barrier (Fig. 2). The reaction starts from the initial state where the $H_2$ molecule stands by at a local energy minimum. When the $H_2$ molecule moves toward one moiety of the dimer, the reaction curve goes up in energy and reaches its maximum at the transition state, where the $H_2$ molecule splits and the two H atoms bond to a Si atom adjacent to the vacancy and one back oxygen atom of the Si atom, respectively. It should be noted that there are a three-coordinated oxygen and a five-coordinated silicon simultaneously in the transition state. It has been shown by first-principles calculations that protons ($H^+$) tend to attach to oxygen bridges in silica, leading to three-coordinated oxygen atoms, and that $H^-$ ions tend to attach to silicon atoms, leading to five-coordinated silicon atoms.[37] The negatively-charged five-coordinated Si atom is unstable due to the positively-charged Si–Si bond adjacent to it, and then the transition state further relaxes to the final state where a Si dangling bond is projecting toward a H–Si group. By this reaction, a proton is released and a Si dangling bond is also created, which can be correlated to the fact that both oxide and interface traps may increase with the increasing hydrogen exposure.[6] It should be noted that the released proton attaches to one oxygen bonded to the dangling bond Si, which lowers the total energy as shown by first-principles calculations.[16]

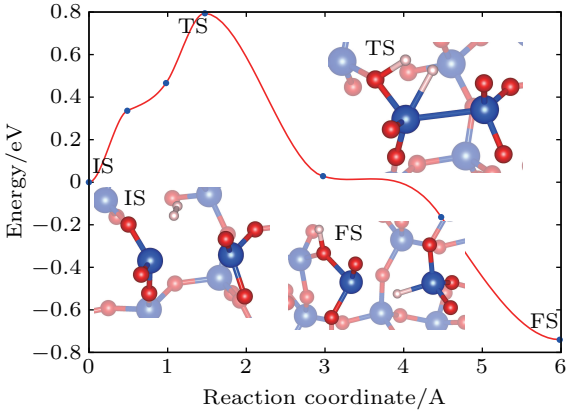



**Fig. 2.** (color online) The reaction curve of $H_2$ dissociating at the dimer configuration. The structures of the initial, transition, and final states are illustrated in the insets.

It is worthwhile to point out that the reaction details revealed by this work are very different from those given in Ref. [17]. According to Ref. [17], the $H_2$ molecule first hydrogenates the dimer configuration in $SiO_2$, leading to the transition state in which two adjacent H–Si groups share a positive charge, and then one of the H–Si bonds dissociates to give a proton, which migrates and attaches to a nearby oxygen bridge. It is obvious that the reaction in a-$SiO_2$ can be divided into three major steps corresponding to the three peaks in the reaction curve. However, the reaction in quartz is one-step, and then there is only one peak in the reaction curve.

The forward reaction barrier in quartz is 0.79 eV, slightly higher than that in a-$SiO_2$. The rate constant of the reaction estimated from the barrier is approximately 0.3 $s^{-1}$ at room temperature (300 K), implying that the reaction takes place rather quickly, possibly in seconds. More than that, while the reaction in a-$SiO_2$ is shown to be endothermic by first-principles calculations,[17] the reaction in quartz is exothermic, and the final-state energy is lower than the initial state energy by 0.74 eV. This implies that the reaction tends to generate protons in quartz instead of annihilating them in a-$SiO_2$.

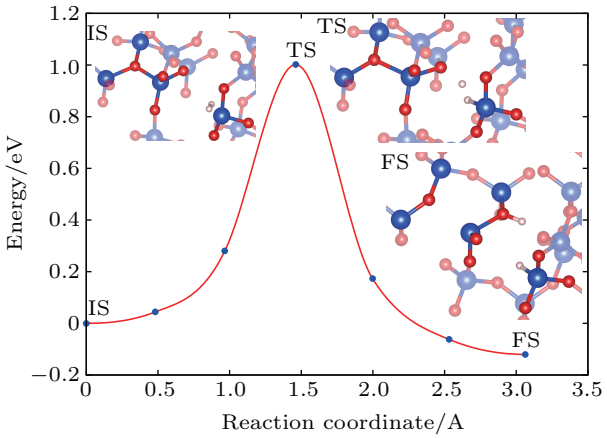



**Fig. 3.** (color online) The reaction curve of molecular hydrogen dissociating at the puckered configuration of the positively charged oxygen vacancy. The structures of the initial, transition, and final states are illustrated in the insets.

The dissociation of $H_2$ molecules at the puckered $E_1'$ centers is also investigated, and the reaction curve is plotted in Fig. 3. The reaction starts from the initial state where the $H_2$ molecule is approaching the Si dangling bond of the puckered configuration. When the reaction goes up, the $H_2$ molecule gradually interacts with the dangling bond and dissociates. At the transition state, one of the H atoms passivates the Si dangling bond and the other is neutral and free in the interstitial space. The neutral free H atom then attaches to one oxygen atom of the puckered moiety of the center, and triggers the collapse of the puckered moiety with a charge transfer. At the final state, the bond between the puckered Si atom and its back oxygen is broken, and the hole trapped at the three-coordinated oxygen in the puckered moiety transfers to the oxygen attached to the H atom. By this reaction, a proton is released and a Si dangling bond is also created. In addition, the released proton attaches to one oxygen atom bonded to the dangling bond Si atom. In fact, the final state of the reaction at the puckered configuration is almost identical to that at the dimer, except that the dangling bond is projecting forward the H–Si group in the former but backward in the latter.

It should be noted that the details of the reaction simulated by this work are quite different from those given in Ref. [17]. According to Ref. [17], the $H_2$ molecule is split by an $sp^2$ hybridized Si atom and an oxygen atom, leading to the final state in which the released proton is attached to one oxygen not bonded to the dangling bond Si atom.

The forward barrier of the reaction in quartz is 1.00 eV, about twice that in a-$SiO_2$. The rate constant estimated from the forward reaction barrier is approximately $1 \times 10^{-4}$ $s^{-1}$ at 300 K, implying that the reaction takes place rather slowly. Given the concentration of the puckered configuration is about a tenth that of the dimer,[38–40] it can be estimated that the proton production rate at puckered configurations is lower than that at dimers by four orders of magnitude. The final state is lower than the initial state by 0.12 eV, so the reaction is exothermic. This implies that the reaction at puckered configurations tends to release protons instead of annihilating them. From the reaction energies at dimer and puckered configurations and the fact that the concentration of puckered configuration is about a tenth that of dimer, it can however be estimated that the proton concentration associated with the $H_2$ dissociation at puckered configurations is lower than that at dimers by five orders of magnitude at equilibrium at 300 K. This implies that the $H_2$ dissociation at dimers can be the dominant reaction that generates protons from $H_2$ molecules.

### 3.3. Hydrogenated oxygen vacancies

The $H_2$ dissociation mechanism can generate protons efficiently, as long as there is a sufficient supply of $H_2$ molecules. However, radiation can still induce interface traps, even if excess $H_2$ is absent in the oxide.[5] This can be partly attributed to the radiolytic hydrogen molecules from hydroxyl groups,[41] and partly to other mechanisms of proton release, such as the dissociation of hydrogenated oxygen vacancies. Before exploring these reactions, we specify the structures and properties of these defects in neural charge state.

When an oxygen vacancy is singly hydrogenated, there are two different resulting structures depending on the projection of the Si dangling bond. In the so-called $E_2'$ centers, the Si dangling bond is projected backward to the H–Si group as shown in the inset of Fig. 4(a), where the spin-density is well localized on the dangling bond Si atom except that a small amount diffuses on the three oxygen atoms bonded to the Si atom and one nonbonding back oxygen. The back-projected

Si dangling bond will be well isolated if there is no back oxygen atom close to the dangling bond in a-$SiO_2$. This structure is thus proposed for the $E'_\beta$ observed in EPR.[42–44] In the so-called $E'_4$ centers, the Si dangling bond is however projected toward the H–Si group as shown in the inset of Fig. 4(b), where two Si atoms and one H atom are bonded by two electrons and asymmetrically share one extra spin. The calculated DOS shows that the occupied defect states are 3.34 eV and 4.20 eV above the VBM in the $E'_2$ and $E'_4$ centers, respectively. It should be noted that $H_2$ dissociations at dimers and puckered configurations lead to the $E'_4$ and $E'_2$ centers, respectively.

Two doubly-hydrogenated oxygen vacancies are obtained by further passivating the $E'_2$ and $E'_4$ centers (Fig. 4(c) and 4(d)). They are nonmagnetic and silent in EPR measurements. The calculated DOS shows that the occupied defect states of the $E'_2$ and $E'_4$ centers induce shallow defect states in the bandgap, which lie at 0.24 eV and 0.52 eV above the valence band, respectively.

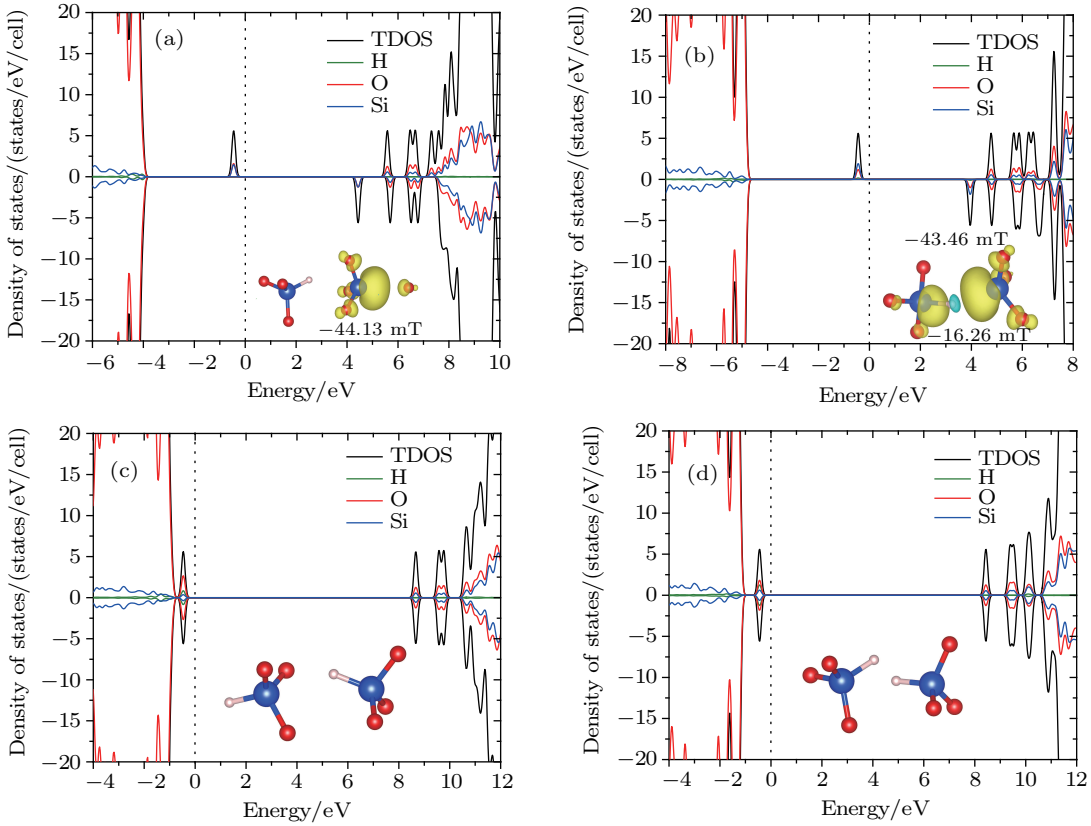



**Fig. 4.** (color online) The calculated DOS of (a) the $E'_2$ center, (b) the $E'_4$ center, (c) the doubly hydrogenated oxygen vacancy derived from the $E'_2$ center, and (d) the doubly hydrogenated oxygen vacancy derived from the $E'_4$ center. The structure and spin density of the centers are illustrated in the insets, respectively.

### 3.4. Proton release reactions of hydrogenated oxygen vacancies

The hydrogenated oxygen vacancies may dissociate to give protons once positively charged. These reactions are simulated by the NEB calculations, and the initial states are given by the structure optimizations of the positively charged hydrogenated centers. We first consider the dissociations of the positively charged $E'_2$ and $E'_4$ centers. Although the neutral $E'_2$ and $E'_4$ centers have different structures, the positively charged centers both relax to the hydrogen bridge configuration $H_B^+$, which is the initial state of the dissociation (Fig. 5). The forward reaction barrier is as high as 2.25 eV, corresponding to a rate constant of $1 \times 10^{-25}$ $s^{-1}$ at room temperature, which implies that the dissociation is almost impossible. The high barrier is due to the strong three-center bond that stabilizes the initial state, the $H_B^+$ configuration. In fact, the $H_B^+$ configuration can be obtained by removing the extra spin on the nonbonding orbital from the neutral $E'_4$ center. It can thus be estimated from the calculated DOS of the $E'_4$ center that the $H_B^+$ configuration is lower than the neutral $E'_4$ center in energy by about 4 eV. The strong three-center bond is interrupted in the transition state, and then the H atom moves from the middle of the $H_B^+$ configuration to one side of the vacancy, which leads to the high forward reaction barrier. The final state however is rather low in energy because of the hydronium-like structure associated with the released proton and the neutral Si–Si bond over the vacancy, but is higher than the initial state by about 0.27 eV. The dissociation is thus an endothermic reaction, which is more likely to trap protons instead of freeing them.

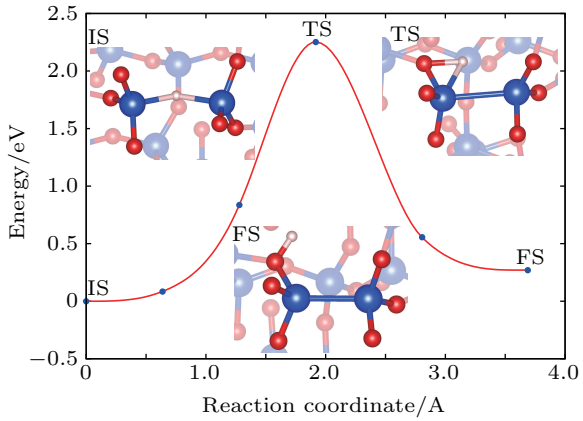



**Fig. 5.** (color online) The reaction curve of the proton liberated from the positively charged $H_B^+$ configuration. The structures of the initial, transition, and final states are illustrated in the insets.

In addition to the $H_B^+$ configuration, there is another possible configuration for the singly hydrogenated oxygen vacancy in the positive charge state, that is, the singly hydrogenated $E_1'$ configuration. In this configuration, the dangling bond in the puckered configuration is passivated by hydrogen, and the puckered moiety stays untouched (Fig. 6). Taking this configuration as the initial state, the dissociation takes place in two major steps. The singly hydrogenated $E_1'$ configuration first converts to the $H_B^+$ configuration by overcoming a low barrier of 0.5 eV associated with the transition state, where the puckered moiety collapses to give a three-coordinated Si atom with $sp^2$ hybridization. The intermediate $H_B^+$ configuration then dissociates to give a proton with a high barrier. It should however be noted that the reverse barrier of the first step is as low as 0.25 eV, and the singly hydrogenated $E_1'$ configuration is lower than the $H_B^+$ configuration in energy by about 0.25 eV. This implies that the $H_B^+$ configurations, generated from the $E_2'$ and $E_4'$ centers, should dominantly take the reverse reaction and convert to the singly hydrogenated $E_1'$ configurations, instead of releasing protons.

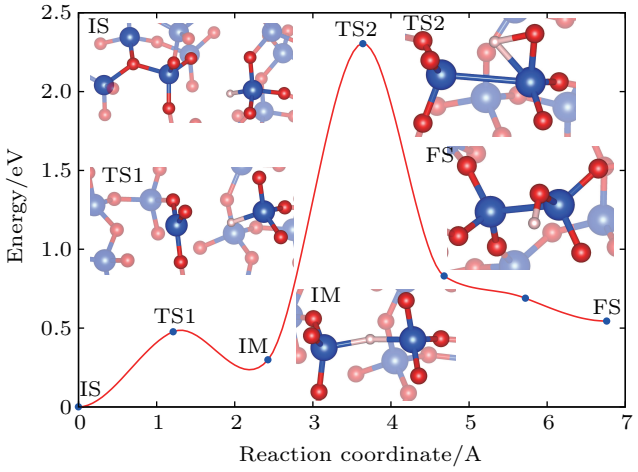



**Fig. 6.** (color online) The reaction curve from the initial state (IS), the singly hydrogenated $E_1'$ configuration, to the final state (FS), the neutral oxygen vacancy with the proton dissociated and attached to a nearby oxygen atom like hydronium, via the intermediate state (IM), the $H_B^+$ configuration.

Although the singly hydrogenated $E_1'$ configuration is lower than the $H_B^+$ configuration in energy, its generation does depend on the back oxygen atom, which is guaranteed to be there in quartz by the crystal structure but might not be there in a-$SiO_2$ due to amorphousness. Thus, some singly hydrogenated oxygen vacancies may convert to and stay at the $H_B^+$ configurations after trapping holes. The hydrogen atom in the $H_B^+$ defect is located asymmetrically between the two Si atoms with the Si–H bond lengths of 1.64 Å and 1.69 Å, respectively, and the Si–H–Si bond angle is 148.41°, in agreement with the previous calculations.[35] The $H_B^+$ configuration induces a series of unoccupied defect states close to the conduction band minimum (CBM) of quartz, the lowest of which is 7.61 eV above the quartz VBM (Fig. 7). Assuming that the Si VBM is aligned at 4.5 eV above the $SiO_2$ VBM, it can be estimated that the defect states are above the Si CBM. The $H_B^+$ configuration is thus stable for a technically meaningful Fermi level, and can be a deep hole trap in a-$SiO_2$.[45]

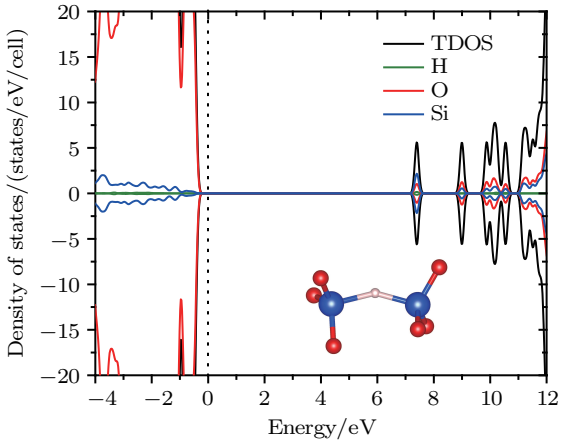



**Fig. 7.** (color online) The atomic and electronic structure of the positive hydrogen bridge ($H_B^+$) configuration.

The dissociations of the doubly hydrogenated oxygen vacancies are investigated in addition to those of the singly hydrogenated ones. The reaction curve of the doubly hydrogenated vacancy derived from the $E_2'$ center is plotted in Fig. 8, where there is no barrier. This implies that the vacancy can readily release a proton by structure relaxation after trapping a hole. In this reaction, the hydrogen atom on the silane group pointing outward from the vacancy gets close and then bonds to one back oxygen atom, forming a hydronium-like structure, and captures the positive charge on the three-coordination oxygen atom. Facilitated by the back oxygen, the dissociation is barrierless and exothermic with a reaction energy of −0.60 eV. Both the barrierless and exothermic characters strongly recommend that this reaction can serve as the dominant mechanism of proton release when the concentration of $H_2$ molecules is low. A caution however should be taken that the back oxygen might not be there in a-$SiO_2$ due to amorphousness.

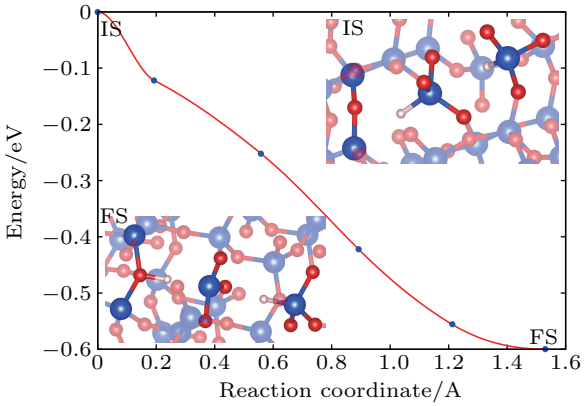



**Fig. 8.** (color online) The reaction curve of the dissociation of doubly hydrogenated oxygen vacancy derived from the $E_2'$ center that releases a proton.

The dissociation of the doubly hydrogenated oxygen vacancy derived from the $E_4'$ center is also simulated in Fig. 9, and there is an obvious barrier in the reaction curve unlike the case of doubly hydrogenated vacancy derived from the $E_2'$ center. In the initial state, the vacancy is positively charged, resulting in a smaller distance between two hydrogen atoms than that in the neutral charge state. The reaction curve goes up in energy when one hydrogen atom is dissociating from a silane group, and reaches the peak associated with the transition state, where the proton is completely freed and a Si dangling bond is created. The freed proton then moves toward and finally attaches to one oxygen atom bonded to the dangling bond Si atom, which is a specific low-energy in quartz.[16] It is noted that the hydrogen atom that initially passivates one of the Si atoms surrounding the vacancy finally turns to forming a Si–H bond with the other Si atom through experiencing the Si–H–Si configuration. The forward reaction barrier of the dissociation is 0.81 eV, from which the rate constant is estimated to be 0.15 $s^{-1}$ at room temperature. This implies that the dissociation can take place rather quickly, within seconds. The reaction however is endothermic with a reaction energy of 0.12 eV, from which it can be estimated that the product concentration is about one percent of the reactant concentration at equilibrium at room temperature. In fact, the reverse reaction is more likely to take place, by which a free proton is captured and fixed into a silane group.

Summarizing the dissociations of the hydrogenated oxygen vacancies in quartz, there is only one reaction, the dissociation of the doubly hydrogenated oxygen vacancy derived from the $E_2'$ center that is characterized of low activation barrier and exothermicity. In addition, the doubly-hydrogenated defects are expected to be present in concentrations ten times larger than the singly-hydrogenated defects.[19] Therefore, the doubly hydrogenated oxygen vacancies derived from the $E_2'$ centers may serve as the dominant proton sources in quartz. A caution however should be raised, that the back oxygen facilitating the dissociation might not be there in a-$SiO_2$ due to the amorphousness.

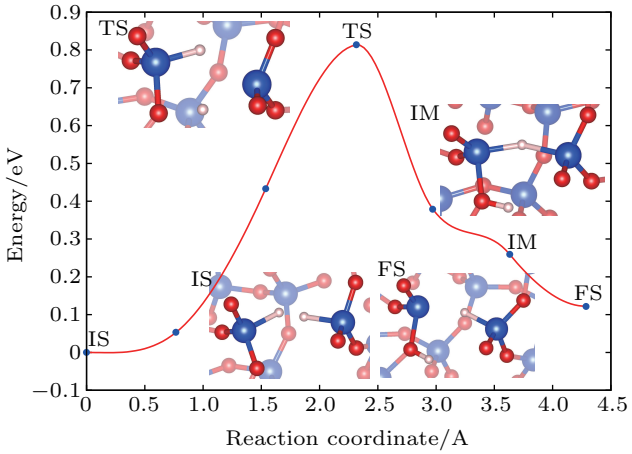



**Fig. 9.** (color online) The reaction curve of the dissociation of the doubly hydrogenated oxygen vacancy derived from the $E_4'$ center that releases a proton.

## 4. Conclusion

The first-principles calculations have been performed to investigate the reactions that probably release protons in $\alpha$-quartz. The dissociations of $H_2$ at the dimer and puckered configurations are simulated for the situation that the concentration of molecular hydrogen is sufficiently high. The calculated reaction curves show that the dissociation at the dimer configuration has a lower reaction barrier and a larger exothermic reaction energy than that at the puckered configuration. Given that the concentration of the dimer configuration is about ten times that of the puckered configuration, we conclude that the dissociation of $H_2$ molecules at the dimer configurations should be the dominant mechanism accounting for proton production when there is plenty of molecular hydrogen. The dissociations of the hydrogenated oxygen vacancies have also been studied for the situation that molecular hydrogen is absent. The calculated reaction curve shows that the singly hydrogenated vacancies need to climb over a high energy barrier to give protons, and that the reaction is endothermic because of the low energy of the positive hydrogen bridge configuration in the initial state. In addition, the positive hydrogen bridge can further lower its energy by puckering. The dissociations of the doubly hydrogenated vacancies however sensitively depend on the projections of the silane groups. The hydrogen atom can dissociate without an energy barrier from the silane group projecting toward the back oxygen atom in the vacancy derived from the $E_2'$ center. The dissociation of the vacancy derived from the $E_4'$ center has a moderately high barrier and is endothermic, because both silane groups are projecting toward the center of the vacancy. The reactions investigated here can be associated with the proton generation at high and low concentrations of molecular hydrogen. The specific details of these reactions are revealed, providing an insight to proton re-

lease mechanism in silicon dioxide, the most widely applied oxide in microelectronics.

## References


[1] Fleetwood D M, Pantelides S T and Schrimpf R D 2008 *Defects in Microelectronic Materials and Devices* (Boca Raton: CRC Press) pp. 215–238

[2] Pacchioni G, Skuja L and Griscom D L 2000 *Defects in $SiO_2$ and Related Dielectrics: Science and Technology* (New York: Springer Science & Business Media) pp. 529–556

[3] Devine R A 1988 *The Physics and Technology of Amorphous $SiO_2$* (New York: Plenum Press) pp. 259–265

[4] Deal B E and Helms C R 1993 *The Physics and Chemistry of $SiO_2$ and the Si-$SiO_2$ Interface* (New York: Springer Science & Business Media) pp. 455–457

[5] Pease R L, Dunham G W, Seiler J E, Platteter D G and Mcclure S S 2007 *IEEE Trans. Nucl. Sci.* **54** 1049

[6] Chen X J, Barnaby H J, Vermeire B, Holbert K, Wright D, Pease R L, Dunham G, Platteter D G, Seiler J, McClure S and Adell P 2007 *IEEE Trans. Nucl. Sci.* **54** 1913

[7] Batyrev I G, Hughart D, Durand R, Bounasser M, Tuttle B R, Fleetwood D M, Schrimpf R D, Rashkeev S N, Dunham G W, Law M and Pantelides S T 2008 *IEEE Trans. Nucl. Sci.* **55** 3039

[8] Rashkeev S N, Fleetwood D M, Schrimpf R D and Pantelides S T 2004 *IEEE Trans. Nucl. Sci.* **51** 3158

[9] Oldham T R and McLean F B 2003 *IEEE Trans. Nucl. Sci.* **50** 483

[10] Rashkeev S N, Fleetwood D M, Schrimpf R D and Pantelides S T 2001 *Phys. Rev. Lett.* **87** 165506

[11] Pease R L, Adell P C, Rax B G, Chen X J, Barnaby H J, Holbert K E and Hjalmarson H P 2008 *IEEE Trans. Nucl. Sci.* **55** 3169

[12] Fleetwood D M, Schrimpf R D, Pantelides S T, Pease R L and Dunham G W 2008 *IEEE Trans. Nucl. Sci.* **55** 2986

[13] Pantelides S T, Tsetseris L, Rashkeev S N, Zhou X J, Fleetwood D M and Schrimpf R D 2007 *Microelectron. Reliab.* **47** 903

[14] Conley J F and Lenahan P M 1993 *IEEE Trans. Nucl. Sci.* **40** 1335

[15] Conley J F and Lenahan P M 1993 *Appl. Phys. Lett.* **62** 40

[16] Van Ginhoven R M, Hjalmarson H P, Edwards A H and Tuttle B R 2006 *Nucl. Instrum. Methods Phys. Res., Sect. B* **250** 274

[17] Tuttle B R, Hughart D R, Schrimpf R D, Fleetwood D M and Pantelides S T 2010 *IEEE Trans. Nucl. Sci.* **57** 3046

[18] Shen X, Puzyrev Y S, Fleetwood D M, Schrimpf R D and Pantelides S T 2015 *IEEE Trans. Nucl. Sci.* **62** 2169

[19] Rowsey N L, Law M E, Schrimpf R D, Fleetwood D M, Tuttle B R and Pantelides S T 2011 *IEEE Trans. Nucl. Sci.* **58** 2937

[20] Silsbee R H 1961 *J. Appl. Phys.* **32** 1459

[21] Jani M G, Bossoli R B and Halliburton L E 1983 *Phys. Rev. B* **27** 2285

[22] Rudra J K, Fowler W B and Feigl F J 1985 *Phys. Rev. Lett.* **55** 2614

[23] Isoya J, Weil J and Halliburton L 1981 *J. Chem. Phys.* **74** 5436

[24] Vitiello M, Lopez N, Illas F and Pacchioni G 2000 *J. Phys. Chem. A* **104** 4674

[25] Kresse G and Furthmüller J 1996 *Comput. Mater. Sci.* **6** 15

[26] Kresse G and Joubert D 1999 *Phys. Rev. B* **59** 1758

[27] Blöchl P E 1994 *Phys. Rev. B* **50** 17953

[28] Perdew J P, Burke K and Ernzerhof M 1996 *Phys. Rev. Lett.* **77** 3865

[29] Levien L, Prewitt C T and Weidner D J 1980 *Am. Mineral.* **65** 920

[30] Henkelman G, Uberuaga B P and Jónsson H 2000 *J. Chem. Phys.* **113** 9901

[31] Alkauskas A, Broqvist P, Devynck F and Pasquarello A 2008 *Phys. Rev. Lett.* **101** 106802

[32] Stahlbush R E, Mrstik B J and Lawrence R K 1990 *IEEE Trans. Nucl. Sci.* **37** 1641

[33] Stahlbush R E, Edwards A H, Griscom D L and Mrstik B J 1993 *J. Appl. Phys.* **73** 658

[34] Snyder K C and Fowler W B 1993 *Phys. Rev. B* **48** 13238

[35] Blöchl P E 2000 *Phys. Rev. B* **62** 6158

[36] Boero M, Pasquarello A, Sarnthein J and Car R 1997 *Phys. Rev. Lett.* **78** 887

[37] Godet J and Pasquarello A 2005 *Microelectron. Eng.* **80** 288

[38] Sushko P V, Mukhopadhyay S, Mysovsky A S, Sulimov V B, Taga A and Shluger A L 2005 *J. Phys.: Condens. Matter* **17** S2115

[39] Girard S, Richard N, Ouerdane Y, Origlio G, Boukenter A, Martin-Samos L, Paillet P, Meunier J P, Baggio J and Cannas M 2008 *IEEE Trans. Nucl. Sci.* **55** 3508

[40] Lu Z Y, Nicklaw C J, Fleetwood D M, Schrimpf R D and Pantelides S T 2002 *Phys. Rev. Lett.* **89** 285505

[41] Griscom D L 1985 *J. Appl. Phys.* **58** 2524

[42] Griscom D L 1985 *J. Non-Cryst. Solids* **73** 51

[43] Griscom D L 1991 *J. Ceram. Soc. Jpn.* **99** 923

[44] Griscom D L 1984 *Nucl. Instrum. Methods Phys. Res., Sect. B* **1** 481

[45] Godet J, Giustino F and Pasquarello A 2007 *Phys. Rev. Lett.* **99** 126102